CERAMIC MATERIALS FOR NUCLEAR ENERGY APPLICATIONS

# Mesoscale Modeling of High Burn-Up Structure Formation and Evolution in UO$_2$

M. GOMAA ABDOELATEF [ID],[1,4] FERGANY BADRY,[1] DANIEL SCHWEN,[2] CODY PERMANN,[2] YONGFENG ZHANG,[2,3] and KARIM AHMED[1]

1.—Nuclear Engineering Department, Texas A&M University, College Station, TX, USA. 2.—Fuel Modeling and Simulation Department, Idaho National Laboratory, Idaho Falls, ID, USA. 3.—Department of Engineering Physics, University of Wisconsin–Madison, 1500 Engineering Drive, Madison, WI 53706, USA. 4.—e-mail: M.Abdoelatef@tamu.edu

A phase-field model was developed to simulate the high burn-up structure formation and evolution in UO$_2$. The model takes into account the interfacial energies of grain boundaries and bubble surfaces, the strain energy associated with dislocations, and the chemical energy of gas atoms. This enables the model to simulate the formation and growth of sub-grains and bubbles in a self-consistent manner. The model results demonstrate strong effects of dislocation density (its magnitude and distribution), grain boundary energy, and bubble radius and number density on the formation of the sub-grains. For polycrystalline UO$_2$, the model predicts the average size of the recrystallized grains to lie within the range of 0.3–0.5 $\mu$m corresponding to a dislocation density range of $\rho = (2.5 \times 10^{15} - 2.65 \times 10^{15})$ m$^{-2}$ or equivalent to 70–75 GWd/tHM burn-up. These predictions agree reasonably well with data reported in the literature.

## INTRODUCTION

For economic reasons, and in anticipation of the operating conditions of next-generation reactors, nuclear fuels have been continuously tested in high burn-up conditions. Most of these tests have reported the formation of the so-called high burn-up structure (HBS).[1] The HBS exhibits a porous, fine-grained microstructure as opposed to the as-fabricated dense, large-grain microstructure. Initially, the HBS was called the rim structure due to its confinement to the periphery of the fuel pellet in light water reactors, where it was first observed. HBS forms at the rim region of the UO$_2$ pellet due to higher burn-up (above 50 GWd/tHM[1]) and lower temperature (below 1373 K[1]) in this region. The burn-up value at the periphery could be twice as large as in the pellet center. This is caused by the presence of higher Pu concentration resulting from resonance absorption of epithermal neutrons by U$^{238}$.[1–3] Nonetheless, in heterogenous fuels such as MOX, the HBS is not only confined to the rim region but is also distributed among high local burn up locations.[1] That observation pushed the community to abandon the old term rim structure in favor of the more general term high burn-up structure (HBS).[1]

The driving force for HBS formation is the reduction of the strain energy by introducing defect-free new sub-grains at the expense of damaged/deformed grains.[1–4] This reduction offsets the increase of interfacial energy due to the formation of new boundaries. It is well established that the thermal and mechanical properties of nuclear fuels are affected by HBS formation.[1–5] Moreover, HBS also influences the swelling and gas release rates, and hence the overall fuel integrity and performance. Therefore, investigating HBS formation and evolution in nuclear fuels is crucial to improve the overall reactor performance and safety.[1–6] HBS formation has been reported to have both positive and negative effects on fuel performance.[1,7]

Different hypotheses have been introduced to explain the HBS phenomenon.[1–6,8] The main suggested mechanisms are recrystallization and grain subdivision.[1–4,8] In the recrystallization scenario, new sub-grains nucleate and then grow at the expense of damaged grains. On the other hand, for the case of grain subdivision, the spatial rearrangement of dislocations into low-angle boundaries leads eventually to the division of the original large grains into smaller sub-grains.

The main goal of the current communication is to model and simulate the process of HBS formation and evolution in $UO_2$. To that end, we utilize the phase-field method, which is a powerful modeling approach that has been used to investigate different types of phase transformations and microstructure evolution processes in heterogeneous materials.[9] The phase-field method has also been adapted to investigate irradiation effects in nuclear materials.[7,10–13] The phase-field modeling approach has recently been employed to investigate irradiation-induced recrystallization.[14,15] In these studies, the effects of fission rate and grain size on recrystallization kinetics were thoroughly investigated. However, in those models, the nucleation rate, recrystallized grain size, and recrystallized grain shape/morphology are assumed a priori to be based on classical nucleation theory. This limits those models to predict only the kinetics of recrystallization. Moreover, those assumptions directly control both the resultant microstructure and the overall kinetics. Therefore, establishing a general model that relaxes these assumptions is desirable. Other modeling techniques such as rate theory[16,17] and cluster dynamics[18,19] have been utilized to study irradiation-induced recrystallization. While these techniques are capable of predicting the average recrystallization kinetics, they also employ the classical nucleation theory and ignore the heterogeneity of the underlying microstructure.

We introduce here a novel phase-field model for HBS formation and evolution. For simplicity, our model utilizes a continuum dislocation density field instead of resolving individual dislocations. Moreover, HBS formation is modeled here as a phase transition. In particular, the self-arrangement of the dislocations into sub-grains can be treated in a way similar to the classical disorder–order transitions in alloys, with the distinction that the dislocations and not the individual atoms are the ones experiencing the self-organization. This model generalizes the grain growth models[20,21] by adding the stored strain energy contribution associated with dislocations formed under irradiation. Such a generalization makes this model capable of simulating the formation and subsequent growth of recrystallized grains. The effects of the density and distribution of dislocations on the recrystallization kinetics have been thoroughly investigated. Moreover, the influence of gas bubbles on the overall kinetics of HBS formation has also been examined.

This manuscript is organized as follows. We describe in "Phase Field Modeling of HBS Formation" section the phase field model that was implemented to simulate the HBS formation and evolution. Then, the results of the simulations are discussed in "Results and Discussion" section. Lastly, we present the main conclusions of this study in "Concluding Remarks" section.

## PHASE FIELD MODELING OF HBS FORMATION

We treat HBS formation in $UO_2$ as a phase transition without distinguishing between recrystallization and grain subdivision. The model developed here builds on the work by Moelans and others on grain growth, migration of recrystallization boundaries, and formulation of thermodynamically-consistent multi-phase-field models.[22–25] The model is obtained through a transformation of the grand-potential model with a parabolic approximation of the chemical free energy as shown in Ref. 25. The resultant formulation is able to decouple the interfacial properties from bulk properties. This allows us to set the interface width independently from the bulk and interfacial thermodynamic properties, and hence facilitates simulating larger domains at a lower computational cost.[25] The formation of new grains is directly accounted for by adding the strain energy contribution to the free energy and stochastic terms to the kinetic evolution equations.

Here, we use several order parameters to fully describe a typical HBS microstructure as depicted in Fig. 1. In order to achieve that goal, such a set of phase fields (order parameters) must be able to distinguish between three different microstructural features, e.g. deformed grains, recrystallized grains, and bubbles. We use $\rho$ for the dislocation density where $\rho \neq 0$ in a deformed/damaged grain and $\rho = 0$ in a recrystallized grain and inside the bubbles. $c$ is the gas site fraction and $\tilde{c}$ is the normalized gas concentration. The normalized concentration is defined as $\tilde{c} = \frac{c - c^{eq}}{1 - c^{eq}}$, such that it equals 0 in the
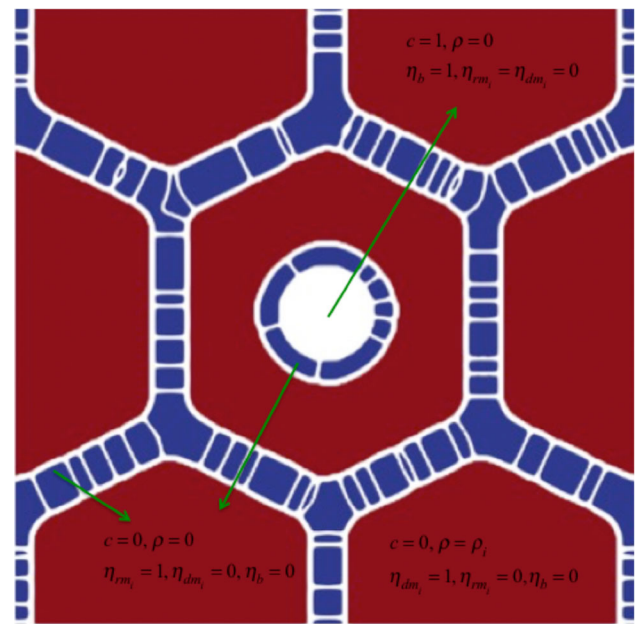


Fig. 1. The phase fields (order parameters) used to describe the HBS microstructure. Damaged grains are shown in red, recrystallized grains are shown in blue, and grain boundaries and bubbles are shown in white (Color figure online).

solid and 1 in the bubble. $c^{\text{eq}}$ is the equilibrium gas concentration in the matrix. In the following, to simplify the notations, we will drop the tilde when we refer to the normalized concentration. $\eta_b$ uniquely identifies the bubble phase such that it equals 1 inside the bubble and 0 everywhere else. The deformed/damaged matrix grains are represented by a set of non-conserved order parameters, $\eta_{\text{dm}_i}$, while the recrystallized matrix grains are represented by another set. $\eta_{\text{rm}_i}$.

Following the theory of gradient thermodynamics suitable for heterogeneous systems,[13] the total free energy of the system is assumed here to have the form:

$$F = \int f_{\text{int}} + f_b^{Th} \text{d}V \qquad (1)$$

In Eq. 1, $f_b^{\text{Th}}$ is the bulk thermodynamic free energy, while $f_{\text{int}}$ represents the interfacial free energy due to bubble (free) surfaces and grain boundaries. The interfacial free energy is given by:

$$f_{\text{int}} = A \begin{bmatrix} 0.25 + 0.25\left(\sum_i \eta_{\text{dm}_i}^4 + \sum_i \eta_{\text{rm}_i}^4 + \eta_b^4\right) - 0.5\left(\sum_i \eta_{\text{dm}_i}^2 + \sum_i \eta_{\text{rm}_i}^2 + \eta_b^2\right) \\ + \gamma_{\text{dm}} \sum_i \sum_{j>i} \eta_{\text{dm}_j}^2 \eta_{\text{dm}_i}^2 + \gamma_{\text{rm}} \sum_i \sum_{j>i} \eta_{\text{rm}_j}^2 \eta_{\text{rm}_i}^2 \\ + \gamma_{\text{rdm}} \sum_i \sum_j \eta_{\text{rm}_j}^2 \eta_{\text{rm}_i}^2 + \gamma_b \eta_b^2 \left(\sum_i \eta_{\text{dm}_i}^2 + \sum_i \eta_{\text{rm}_i}^2\right) \\ + \frac{k}{2}\left[\sum_i |\nabla \eta_{\text{rm}_i}|^2 + \sum_i |\nabla \eta_{\text{dm}_i}|^2 + |\nabla \eta_b|^2\right] \end{bmatrix}$$

$$(2)$$

where $A$, $\gamma_\alpha$ and $k$ are constants that determine the surface and grain boundary energies. This formulation assumes an isotropic surface and grain boundary energies. Nonetheless, the model can be generalized for anisotropic cases in a straightforward manner as in regular grain growth models.[21] The thermodynamic bulk free energy is constructed as:

$$f_b^{\text{Th}} = f^{\text{ch}} + f^{\text{st}} \qquad (3)$$

where $f^{\text{ch}}$ is the chemical free energy and $f^{\text{st}}$ is the stored strain energy associated with dislocations produced at high burn-up.

The strain energy of dislocations is expressed as:

$$f^{\text{st}}\left(\rho, \eta_{\text{dm}_i}, \eta_{\text{rm}_i}, \eta_{\text{p}}\right) = \frac{1}{2} G b^2 \rho(r,t) h_{\text{dm}},$$
$$h_{\text{dm}} = \frac{\sum_i \eta_{\text{dm}_i}^2}{\sum_i \eta_{\text{dm}_i}^2 + \sum_i \eta_{\text{rm}_i}^2 + \eta_b^2} \qquad (4)$$

where $G$ is the shear modulus, $b$ is the length of the Burgers vector, and $h_{\text{dm}}$ represents the fraction of deformed matrix grains in the domain. The effective/average dislocation density can then be calculated as:

$$\rho_{\text{eff}} = \frac{1}{V} \int \rho(r,t) h_{\text{dm}}(r,t) \text{d}V \qquad (5)$$

The dislocation density, $\rho(r,t)$, can vary with space and time. In most simulations here, for simplicity, $\rho(r,t)$ was taken as a constant for all the damaged grains. However, we also investigate the effect of non-uniform dislocation density.

A parabolic approximation of the chemical free energy of the bulk phases is used here, namely:

$$f^{\text{ch}} = B(c - h_b)^2, \quad h_b = \frac{\eta_b^2}{\sum_i \eta_{\text{dm}_i}^2 + \sum_i \eta_{\text{rm}_i}^2 + \eta_b^2} \qquad (6)$$

where $B$ is a constant that sets the value of the chemical free energy and $h_b$ represents the bubble fraction. This specific form eliminates any contribution of the chemical free energy to the interfacial energy, as demonstrated in Ref. 25. Note that this form assumes equal curvatures of the parabolas representing the matrix and the bubble phases. This is acceptable if one assumes the bubbles have their equilibrium pressure, and hence the value of the sole curvature can be used to represent the excess free energy in the matrix due to gas atoms supersaturation. Specifically, we fix the parabola such that the chemical potential calculated from Eq. (6) approximates the exact chemical potential given by the ideal solution form, e.g.:

$$2B\bar{c} = \frac{K_{\text{B}}T}{\Omega} \ln \frac{\bar{c}}{c^{\text{eq}}} \qquad (7)$$

where $K_{\text{B}}$ is the Boltzmann constant, $\Omega$ is the atomic volume, $T$ is the absolute temperature, $\bar{c}$ is the average gas concentration in the matrix, and $c^{\text{eq}}$ is the equilibrium gas concentration in the matrix. The equilibrium gas concentration has a regular form, i.e.,:

$$c^{\text{eq}} = \exp(-E^f / K_{\text{B}}T) \qquad (8)$$

where $E^f$ is the solution energy of a gas atom.

The evolution equations for the phase fields/order parameters can be derived from the principles of irreversible thermodynamics.[13] The non-conserved order parameters evolve according to the Allen–Cahn equations[24] as:

$$\frac{\partial \eta_b}{\partial t} = -L_b \frac{\delta F}{\delta \eta_b}$$
$$= -L_b\left(\frac{\partial f^{\text{int}}}{\partial \eta_b} + \frac{\partial f^{\text{ch}}}{\partial \eta_b} + \frac{\partial f^{\text{st}}}{\partial \eta_b} - k\nabla^2 \eta_b\right) + \xi_b, \quad (9\text{a})$$

$$\frac{\partial \eta_{\text{dm}_i}}{\partial t} = -L_{\text{dm}_i} \frac{\delta F}{\delta \eta_{\text{dm}_i}}$$
$$= -L_{\text{dm}_i}\left(\frac{\partial f^{\text{int}}}{\partial \eta_{\text{dm}_i}} + \frac{\partial f^{\text{ch}}}{\partial \eta_{\text{dm}_i}} + \frac{\partial f^{\text{st}}}{\partial \eta_{\text{dm}_i}} - k\nabla^2 \eta_{\text{dm}_i}\right)$$
$$+ \xi_{\text{dm}_i} \quad \forall i$$

$$(9\text{b})$$

$$\frac{\partial \eta_{\mathrm{rm}_i}}{\partial t} = -L_{\mathrm{rm}_i} \frac{\delta F}{\delta \eta_{\mathrm{rm}_i}}$$

$$= -L_{\mathrm{rm}_i} \left( \frac{\partial f^{\mathrm{int}}}{\partial \eta_{\mathrm{rm}_i}} + \frac{\partial f^{\mathrm{ch}}}{\partial \eta_{\mathrm{rm}_i}} + \frac{\partial f^{\mathrm{st}}}{\partial \eta_{\mathrm{rm}_i}} - k\nabla^2 \eta_{\mathrm{rm}_i} \right)$$

$$+ \xi_{\mathrm{rm}_i} \quad \forall i$$

(9c)

Here, $L_b$ is a constant related to the bubble surface mobility, $L_{\mathrm{dm}_i}$ is a constant related to the boundary mobility of a deformed/damaged matrix grain, $L_{\mathrm{rm}_i}$ is a constant related to the boundary mobility of a recrystallized matrix grain, and $\xi_\alpha$ are stochastic terms that facilitate nucleation of grains or bubbles. In contrast to the Langevin equation, the stochastic terms here not only represent the thermal fluctuations of atoms/particles but they also account for the cutoff of any fast degrees of freedom necessary for deriving coarse-grained free energy. Adding those terms to the evolution equations enables them to explore other evolution paths in the vicinity of the most probable path in the phase space. Using constant mobility coefficients is equivalent to the assumption of isotropic grain boundary and bubble surface mobilities. Nevertheless, the extension to the anisotropic case can be achieved by following the standard approach used before in the models of solidification and grain growth.[13,20,21]

The gas atom concentration is governed by a Cahn–Hilliard-type diffusion equation, e.g.:

$$\frac{\partial c}{\partial t} = \nabla \cdot (M\nabla\mu) + P + \xi_c \qquad (10a)$$

$$\mu = \frac{\delta F}{\delta c} = \frac{\partial f^{\mathrm{ch}}}{\partial c} \qquad (10b)$$

In Eqs. 10a and 10b, $M$ is the chemical mobility of gas atoms, $\mu$ is their chemical potential, $P$ is a source term representing the on-going production of gas atoms due to fission events, and $\xi_c$ is a stochastic term similar to the ones discussed above. The chemical mobility is related to the diffusivity ($D$) through:

$$\frac{\partial^2 f^{\mathrm{ch}}}{\partial c^2} M = D, \qquad (11a)$$

$$2BM = D. \qquad (11b)$$

Using constant mobility here amounts to considering bulk diffusion to be the sole mechanism of gas atom diffusion. However, grain boundary and surface diffusion mechanisms can be added to the model, as in the work of Ahmed. et al.[26,27] on grain growth in porous solids.

The effective dislocation density is prescribed according to a constitutive law. In general, the dislocation density can change with time and position. These dependencies represent the accumulation of radiation damage and the heterogeneity of

damage expected in distinct types of fuels used in different reactor types. For the sake of simplicity, we utilize here an empirical relationship that calculates the average dislocation density for a given burn-up (Bu), e.g.:[6]

$$\log \rho_{\mathrm{eff}} = 2.2 \times 10^{-2} Bu + 13.8 \qquad (12)$$

The deformed grains are assumed to have this dislocation density, while the recrystallized grains are dislocation-free.

The phase-field model parameters are directly related to the thermodynamic and kinetic parameters as follows:[8,25]

$$\gamma_{\mathrm{dm}} = \gamma_{\mathrm{rm}} = \gamma_{\mathrm{rd}} = 1.5 \qquad (13a)$$

$$\left( \frac{\gamma_b}{1.5} \right) = \left( \frac{\gamma_s}{\gamma_{\mathrm{gb}}} \right)^2 \qquad (13b)$$

$$A = \frac{3\gamma_{\mathrm{gb}}}{4\ell} \qquad (13c)$$

$$k = \frac{3}{4}\gamma_{\mathrm{gb}}\ell \qquad (13d)$$

$$L_{\mathrm{dm}} = L_{\mathrm{rm}} = \frac{4M_{\mathrm{gb}}}{3\ell} \qquad (13e)$$

$$L_b = 10\frac{D}{B\ell^2} \qquad (13f)$$

In Eqs. 13a–13f, $\ell$ is the diffuse interface width, $\gamma_{\mathrm{gb}}$ is the grain boundary energy, $\gamma_s$ is the surface energy, and $M_{\mathrm{gb}}$ is the grain boundary mobility. As can be deduced from these equations, it is assumed here that the recrystallized and deformed grains have the same boundary energy and mobility. However, this is not a model restriction, as clear from the equations, but rather a simplification for the lack of data. Equation (13f) guarantees that the bubble surface motion is diffusion-controlled. The grain boundary energy and surface energy of $UO_2$ are taken to be 1.04 J/m$^2$ and $1.8 \pm 0.3$ J/m$^2$, respectively.[28,29] The grain boundary mobility of $UO_2$ is given by:[30]

$$M_b = 9.21 \times 10^{-9} \exp(-2.77 \, \mathrm{ev}/K_B T) \, \mathrm{m}^4/(\mathrm{Js}) \quad (14)$$

The shear modulus and the magnitude of the Burgers vector for $UO_2$ are taken as $G = 73$ Gpa, $b = 0.39$ nm.[6] The interface width was set to 20 nm in all the simulations. A temperature of 1200 K is assumed for all the simulations conducted here.

The model was implemented using the open-source finite-element code MOOSE, which uses its built-in Grain Tracker algorithm[31] to reduce the computational cost. Grain Tracker is an algorithm implemented in MOOSE that allows the using of a few numbers of order parameters to represent a large number of grains, which facilitates performing
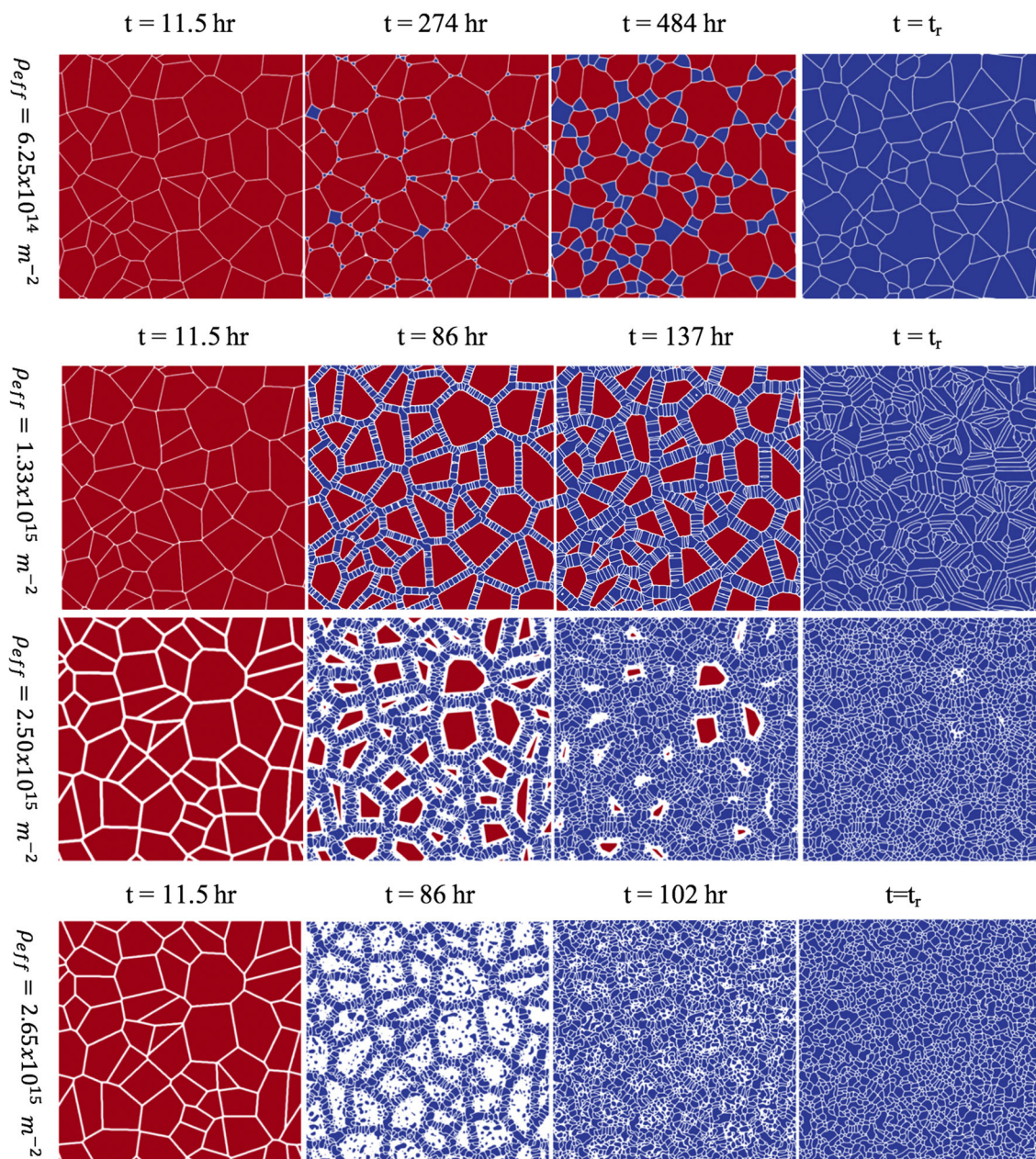
Fig. 2. Effect of dislocation density on irradiation-induced recrystallization in polycrystalline UO$_2$ at 1200 K. The initially damaged grains are presented in red and the recrystallized (dislocation-free) grains in blue. $t_r$ is the time at which recrystallization is complete. The dislocation density increases from the upper row to the lower row. It is clear that the number of recrystallized grains, the average recrystallized grain size, and the morphology of the recrystallized grains are highly influenced by the magnitude of the dislocation density. The recrystallization time ($t_r$) reduces with increasing dislocation density (see Fig. 3) (Color figure online).

large-scale simulations of polycrystalline materials.[31] In 2D simulations, only 8 order parameters are required to represent a few thousand grains. The grain tracker algorithm was utilized here to handle both the deformed grains and the sub-grains (recrystallized grains). To that end, 8 more order parameters were reserved to represent the recrystallized grains ($\eta_{rm_i}$). They are initially zero, and once new grains are formed they are given new identification numbers and represented by one of

the reserved order parameters. Nucleation takes place directly due to the inclusion of the stochastic terms. A uniform random generator with zero mean was used for these stochastic terms. The magnitude of the stochastic terms was found not to appreciably affect the evolution, and it was set to $10^{-3}$ in all the simulations. Lastly, the kinetic evolution equations were solved using the same procedure summarized in Ref. 32. Built-in MOOSE adaptive time and mesh steps were also utilized to speed up the simulations.

## RESULTS AND DISCUSSION

We investigate here the HBS formation and evolution in polycrystalline $UO_2$. All the simulations were conducted in 2-D to reduce the high computational cost. Furthermore, for simplicity, the production and stochastic terms in Eqs. (9a) and (10a) were set to zero, i.e., the nucleation of bubbles was ignored and only their effect on the initiation of HBS transformation was considered. The effects of dislocation density magnitude and distribution, initial grain size, bubble radius and number density were studied systematically. The simulations proved a strong influence of these parameters on the overall kinetics of HBS formation. Moreover, it was demonstrated that these parameters control the resultant microstructure of the HBS, and hence its thermal and mechanical properties.

## Effects of Dislocation Density and Grain Size on HBS Formation

Several simulations were conducted to understand the formation and evolution of HBS in polycrystalline $UO_2$. The simulations utilize a 2-D domain of size $20.48 \times 20.48$ $\mu$m, with an average grid size of 20 nm. The initial size of the damaged grains was varied between 2.9 $\mu$m and 4.1 $\mu$m. For simplicity, in most simulations, all the initial grains were assumed to be damaged and to have the same dislocation density. However, the effect of non-uniform dislocation density was also studied.

First, we investigate the effect of the magnitude of the dislocation density on the process of HBS formation and evolution. This is captured in Fig. 2, which represents snapshots of the HBS formation and evolution. Due to the high
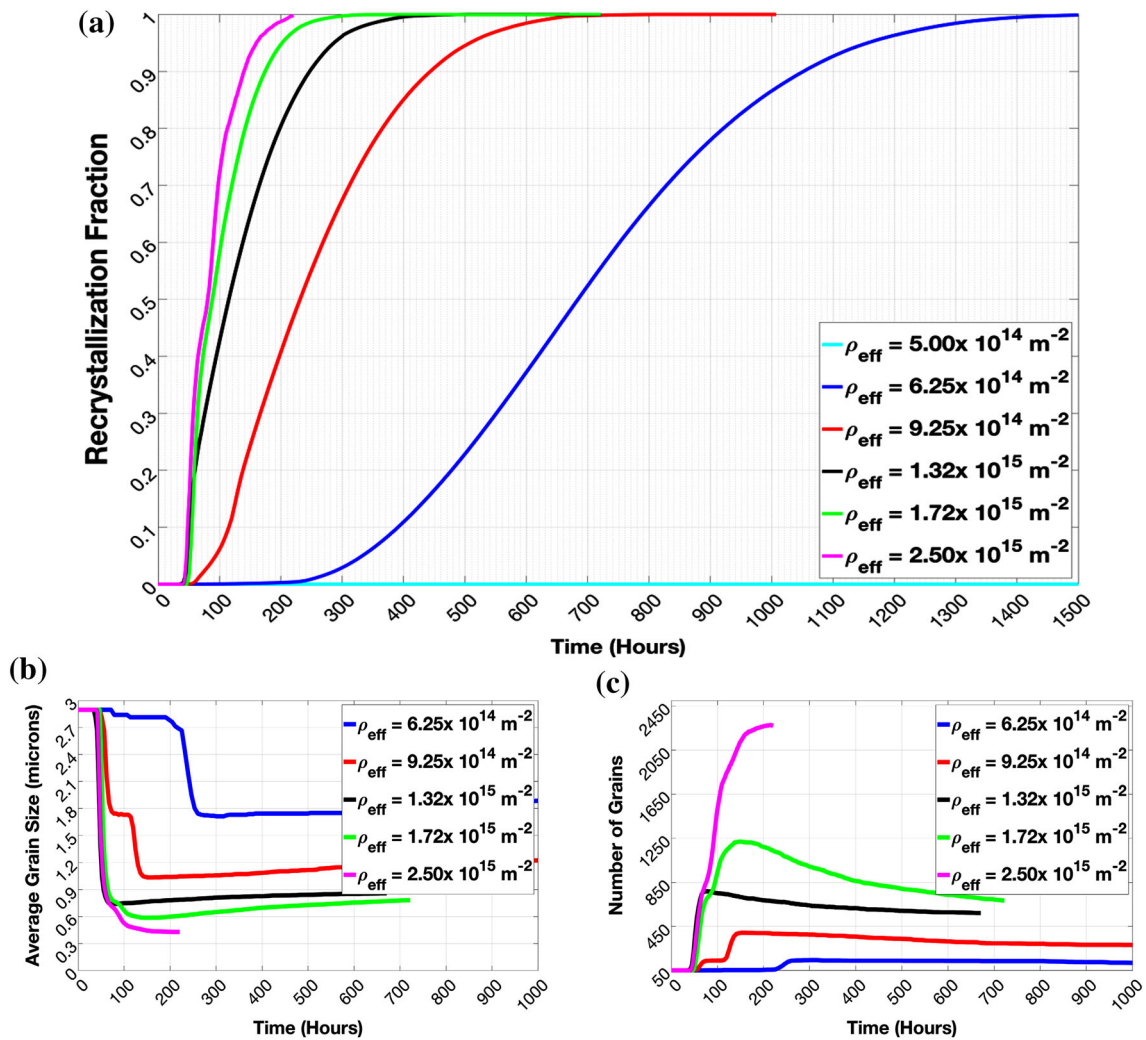


Fig. 3. Effect of dislocation density on the kinetics of recrystallization in polycrystalline $UO_2$ at 1200 K: (a) the increase of the recrystallization fraction (the ratio between the area of the new recrystallized grains and the total domain area) with time; (b) the evolution of the average grain size; and (c) the change in the total number of grains with time.

computational cost, the initial grain size of the damaged grains was set to be 2.9 $\mu$m, which is close to the initial grain size range UO$_2$ pellets (5–10 $\mu$m).[1] As evident from the figure, the value of the dislocation density affects both the size and morphology of the recrystallized grains. A critical dislocation density was found below which no recrystallization takes place. The value of this critical dislocation density is $\rho_{\mathrm{eff}} = 5.17 \times 10^{14}$ m$^{-2}$ or equivalently 41 GWd/tHM burn-up. As the dislocation density increases (from the upper row $\rho_{\mathrm{eff}} = 6.25 \times 10^{14}$ m$^{-2}$ or 45 GWd/tHM burn-up to the lower row $\rho_{\mathrm{eff}} = 2.50 \times 10^{15}$ m$^{-2}$ or 72 GWd/tHM burn-up), the recrystallized grain size decreases and the number of recrystallized grains increases. This is consistent with the fact that the critical radius is inversely proportional to the strain energy difference between the damaged and recrystallized grains. Moreover, as the dislocation density increases, the morphology of the recrystallized grains changes from coarse equiaxed grains at low values of the dislocation density $\rho_{\mathrm{eff}} = 6.25 \times 10^{14}$ m$^{-2}$ to columnar grains at intermediate values $\rho_{\mathrm{eff}} = 1.33 \times 10^{15}$ m$^{-2}$ to fine equiaxed grains at high values $\rho_{\mathrm{eff}} = 2.50 \times 10^{15}$ m$^{-2}$. Furthermore, the heterogeneous nature of recrystallization is sensitive to the magnitude of dislocation density, as shown in Fig. 2. For low values of the dislocation density, recrystallization proceeds only at triple- and higher order-junctions (upper row). At intermediate values, recrystallization also takes place at the grain boundaries (second row). At a high enough dislocation density, new sub-grains form at the boundaries of the just-recrystallized grains (third row). The grain subdivision, where nucleation of new grains can occur inside the bulk of × damaged grains, starts to take place at a higher dislocation density (fourth row). Note that the model correctly reproduces the different morphologies of grains recrystallized at different junctions, e.g. two-, triple-, and higher-order junctions. All these results are consistent with the heterogeneous nucleation theory. This is a major strength of our model where nucleation of recrystallization is treated explicitly and no a priori assumptions on the nucleation rate and sites or the size and morphology of the recrystallized grains are required. The range of dislocation or equivalently burn-up predicted here for HBS formation in UO$_2$ fuel agrees well with the experimental data reported in the literature.[1,6,33,34]

The effect of dislocation density on the overall kinetics of HBS formation in polycrystalline UO$_2$ is quantitatively shown Fig. 3. At very low dislocation density ($\rho_{\mathrm{eff}} = 5.00 \times 10^{14}$ m$^{-2}$) no recrystallization takes place, but a higher dislocation density leads to a shorter incubation time and faster recrystallization kinetics (as evident from Fig. 3a). Moreover, a higher dislocation density results in a larger number of recrystallized grains, and hence smaller average grain size (as can be seen from Fig. 3b).
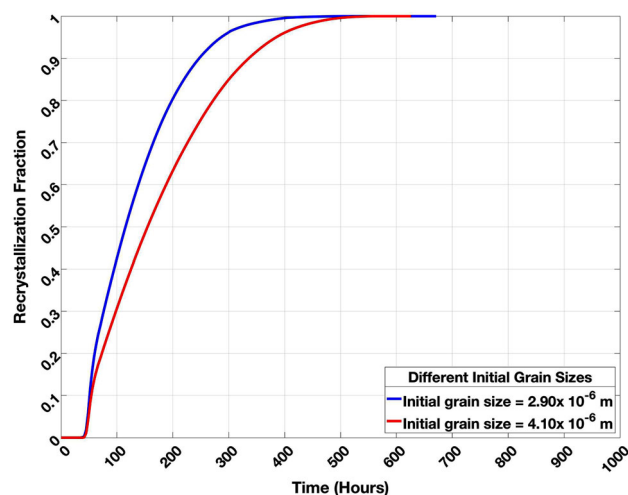


Fig. 4. Effect of the initial grain size on the recrystallization kinetics. Faster recrystallization kinetics is observed for smaller grain sizes due to the higher density of nucleation sites.

This is in good agreement with expectations from the classical nucleation theory.[35] Note that, after recrystallization is complete, regular grain growth, where the number of grains decreases and grain size increases, takes place. For the cases where the resultant microstructure resembles the HBS micrographs, i.e., when it develops uniform and fine grain structures, the recrystallized average grain size was found to lie within the range of 0.3–0.5 $\mu$m corresponding to a range of dislocation densities of $\rho = \left(2.5 \times 10^{15} - 2.65 \times 10^{15}\right)$ m$^{-2}$ (or equivalently a burn-up of 70–75 GWd/tHM). These ranges of grain size and burn-up agree well with the reported values.[1,6,33,34]

We then studied the effect of the grain size of polycrystalline UO$_2$ on the kinetics of HBS formation. The investigation considered two different initial grain sizes of 2.9 and 4.1 $\mu$m at a dislocation density $\rho = 1.33 \times 10^{15}$ m$^{-2}$. The results of these simulations are presented in Fig. 4. As can be concluded from the figure, recrystallization proceeds faster with decreasing grain size. This is due to the fact that the smaller grain size leads to a higher grain boundary area per unit volume, and hence more preferable nucleation sites. Moreover, the trend predicted here agrees with the experimental date reported for UO$_2$.[6,33,34]

**Effect of the Distribution of Dislocation Density**

In the simulations above, it was assumed that the dislocation density is uniform and constant in all grains. However, this is unrealistic in most situations. For instance, under a non-uniform applied mechanical load or irradiation, the heterogeneous distribution of dislocations is expected. For UO$_2$ pellets, it is known that irradiation damage is more pronounced at the periphery than in the center of the pellet. That is due to the difference in the fission
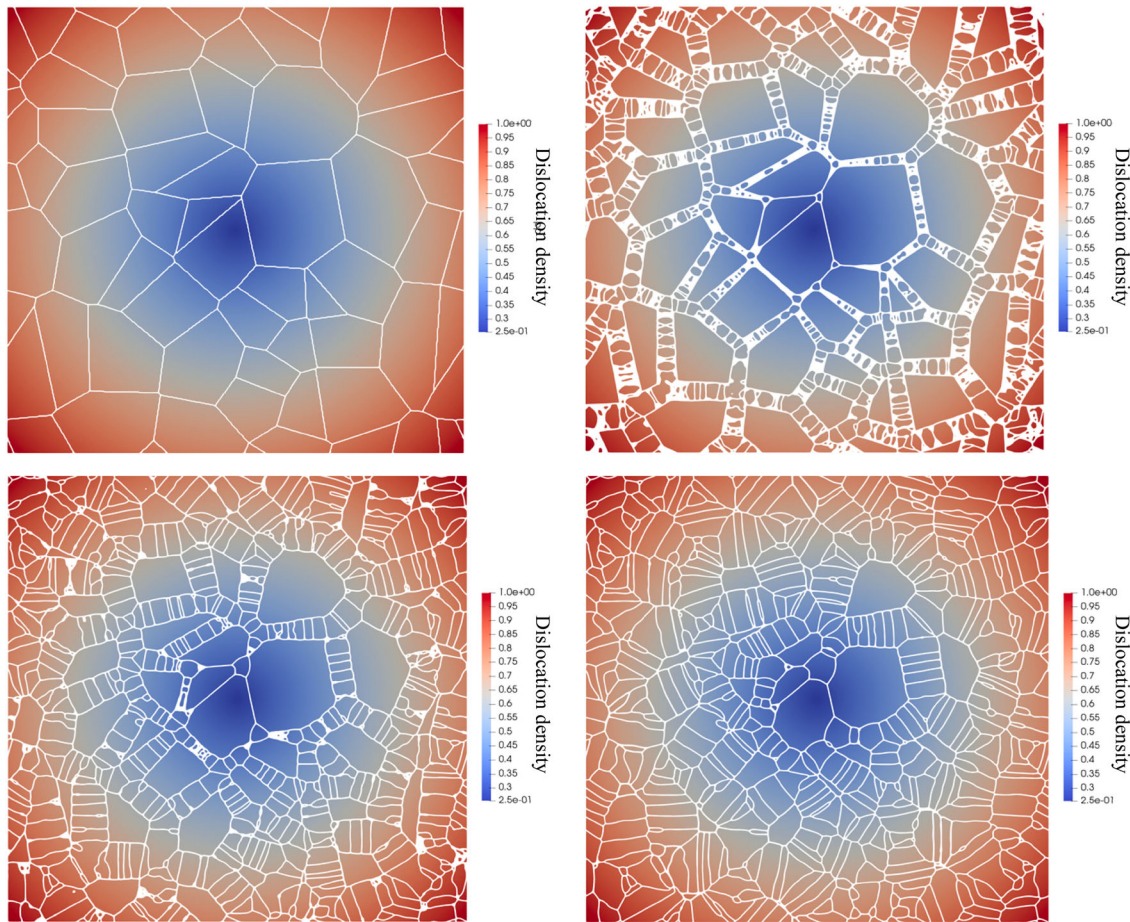
Fig. 5. Simulation of HBS formation in a UO$_2$ pellet. The dislocation density changes radially, i.e., it is lowest at the center and highest at the periphery (see text for exact numbers). Only the grain boundaries and the initial dislocation distribution are shown here for better visualization. Time progresses from top left to bottom right. Note the change in the recrystallized grain size and morphology along the radial direction.

density between those regions. Additionally, the high temperature at the center leads to the annealing of defects. i.e., irradiation damage and recovery take place almost simultaneously at the center of the pellet. Moreover, the stresses arising from the temperature gradient across the pellet center also contribute to the heterogeneity of irradiation damage. Hence, it is expected that the dislocation density will be higher at the periphery than at the center.

We investigate the effect of non-uniform dislocation density by assigning a spatially dependent dislocation density. To approximate the distribution of dislocations in UO$_2$ pellets, we assign a linear profile for the dislocation density along the radius. This is shown in Fig. 5 which represents the HBS formation in polycrystalline UO$_2$ pellets. At the center of the domain, the dislocation density was set to $\rho = 6.25 \times 10^{14}$ m$^{-2}$ (0.25 in the figure as a non-dimentionalized value). The dislocation denisty attained its maximum value $\rho = 2.5 \times 10^{15}$ m$^{-2}$ (1.00 in the figure as a non-dimensionalized value) at the corners of the domain. As can readily be inferred from the figure, the non-uniform

distribution of dislocations leads in turn to a heterogeneous HBS. The recrystallized grain size, orientation, and morphology change drastically along the radius. This is consistent with the above results which demonstrated a strong effect of the value of the dislocation density. This will eventually results in non-uniform mechanical and themal properties along the radius, as has been reported before.[1]

**Effect of Gas Bubbles on the Kinetics of HBS Formation**

We turn our attention to the effect of bubbles on the kinetics of recrystallization in polycrystalline UO$_2$. It has been reported several times that bubble formation often precedes recrystallization during HBS formation in UO$_2$. Moreover, it is well known that second-phase particles in general strongly influence the overall kinetics of both recrystallization and grain growth in materials. On the one hand, they act as nucleation sites, leading to enhanced kinetics of recrystallization. On the other hand, they also act as pinning sites for the grain boundaries, resulting in hindered grain growth
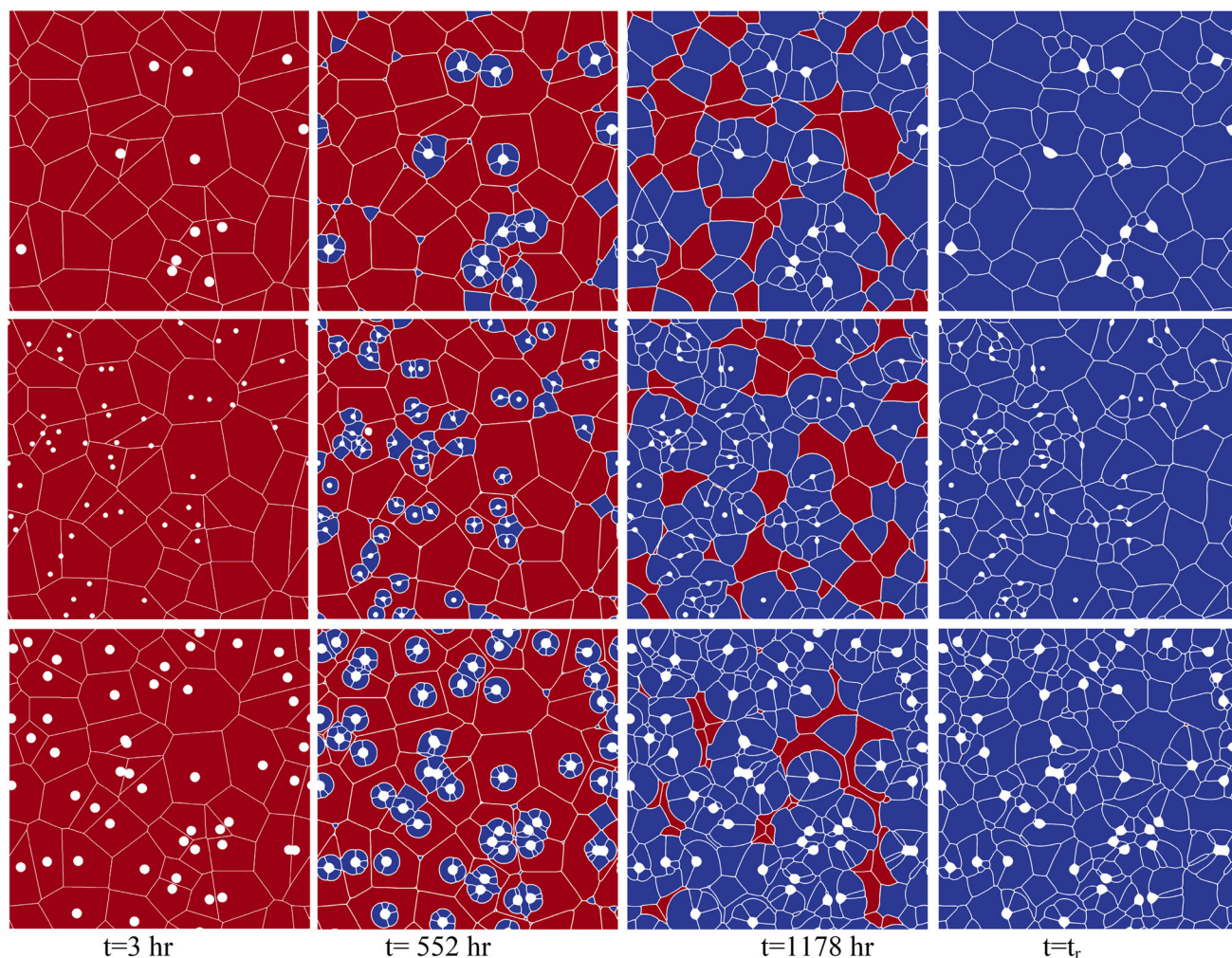
Fig. 6. Effect of gas bubbles on the recrystallization kinetics in polycrystalline UO$_2$ at 1200 K. The first and second rows have the same bubble area fraction. The second and third rows have the same number of bubbles. In all configurations, bubbles tend to accelerate the overall kinetics of recrystallization by providing extra nucleation sites. It is worth noting that grains recrystallized at the bubble surface have different morphologies from those at grain junctions. Note that the bubble morphology changes during the evolution to establish the equilibrium dihedral angle at the bubble tips, i.e., the equilibrium bubble morphology depends on the number of connected grain boundaries. Moreover, the model also captures bubble merging (coarsening) during grain growth (see the last column).

kinetics. To investigate the effect of bubbles on HBS formation in UO$_2$, we performed several simulations with different bubble configurations. The results of these simulations are summarized in Figs. 6, 7, and 8.

Snapshots of HBS formation and evolution are shown in Fig. 6. The number of bubbles and bubble radii were varied to investigate their effects on the process. The initial grain size of 2.9 $\mu$m and a relatively low dislocation density of $\rho = 6.25 \times 10^{14}$ m$^{-2}$ were used. As evident from Fig. 6, the presence of bubbles enhances the kinetics of recrystallization in all cases. It is worth noting that the model correctly reproduces the different equilibrium morphologies of the bubbles and the recrystallized grains. The equilibrium morphology is determined through the establishment of the equilibrium dihedral angle at the bubble/grain tips/triple-junctions. Moreover, the model predicts that the grains

recrystallized near the bubbles tend to wrap around the surface of the bubbles which act as a surface defect, and hence a preferred nucleation site. This was observed in experimental micrographs of HBS.[5,6] Furthermore, the model can also concurrently simulate grain growth and particle coarsening if simulations were to run for longer times, as in Refs. 26 and 32.

The effects of gas bubbles on the overall kinetics of recrystallization in polycrystalline UO$_2$ are quantitatively summarized in Figs. 7 and 8. Figure 7 represents the recrystallization rates at different dislocation densities for two distinct bubble configurations with the same area fraction. Figure 8 shows the recrystallization rates at different dislocation densities for two distinct bubble configurations with the same radius and different number density. As represented in the figures, the recrystallization rate increases with bubble number
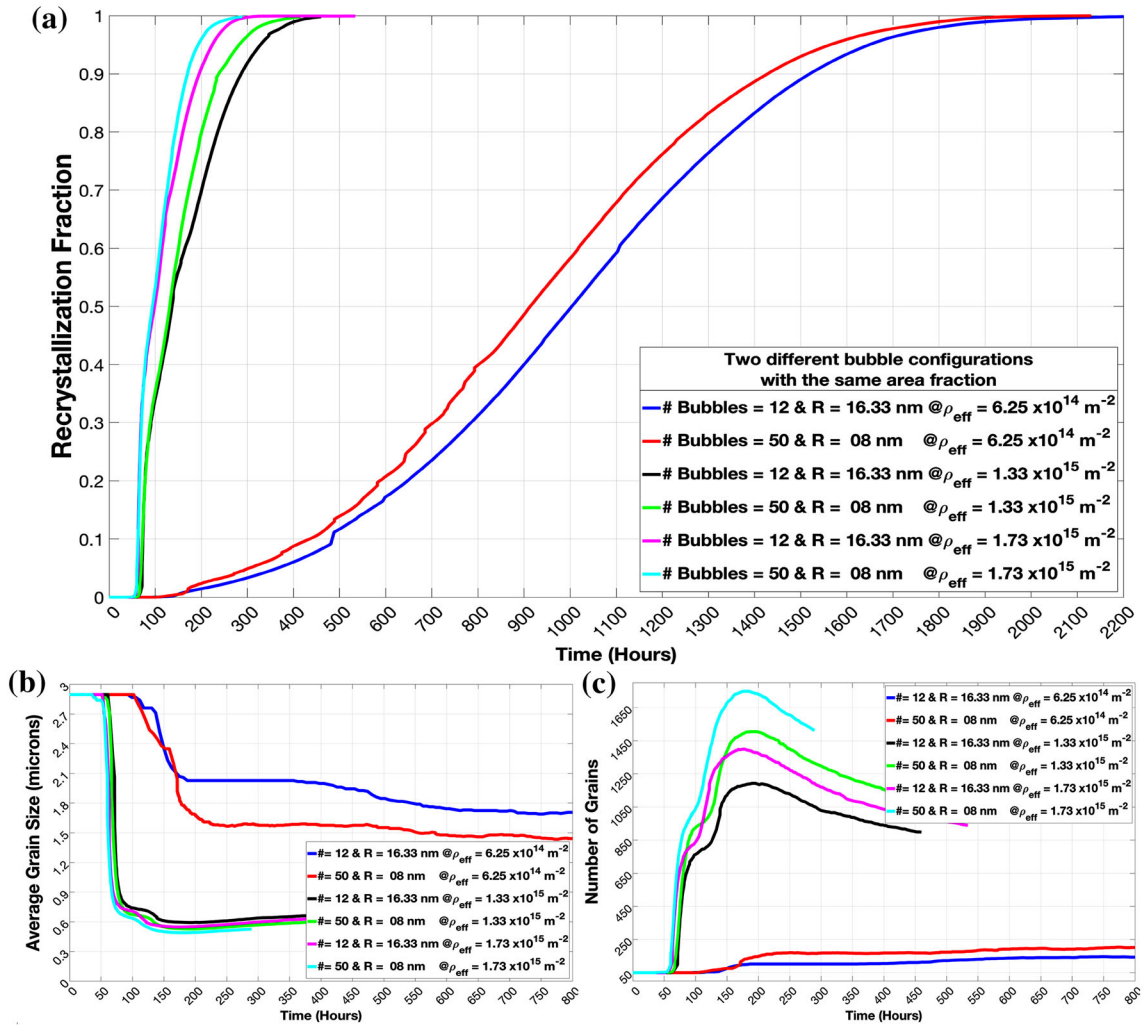
Fig. 7. Effect of gas bubbles on (a) the recrystallization kinetics in polycrystalline O$_2$, (b) average grain size and (c) number of grains. Two different bubble configurations with the same area fraction at different dislocation densities were considered. In all cases, gas bubbles increase the recrystallization rate. This increase is more pronounced at lower dislocation densities. For the same bubble area fraction and dislocation density, configurations with the higher number of bubbles recrystallize faster.

density. The enhancement is more pronounced at lower dislocation densities. This is consistent with the fact that bubbles provide extra nucleation sites for recrystallization to take place. The effect of the bubble radius was also studied but was found to be negligible compared to the number density. Nonetheless, the effect of bubble radius is expected to have a more pronounced effect on the later grain growth kinetics (after recrystallization is complete), as we have demonstarted in previous studies.[26,27,32]

## CONCLUSION

A quantitative phase-field model was introduced to investigate high burn-up structure formation and evolution in polycrystalline UO$_2$. The model directly simulates the nucleation of recrystallization, eliminating the need for making a priori assumptions

and implementing separate algorithms to model the formation of sub-grains. The model accounts for the effects of the magnitude and distribution of dislocations on the HBS. In addition, the model considers the influence of bubbles on HBS formation and evolution. The kinetic evolution equations of the model were solved using a fully coupled and fully implicit scheme implemented in the MOOSE framework.

The simulations showed that the magnitude and distributions of dislocations and bubble number density control the overall kinetics of HBS formation. Moreover, these factors also determine the resultant microstructure of the HBS, and hence its physical properties. The model prediction for the threshold dislocation density related to the HBS formation was found to be in good agreement with
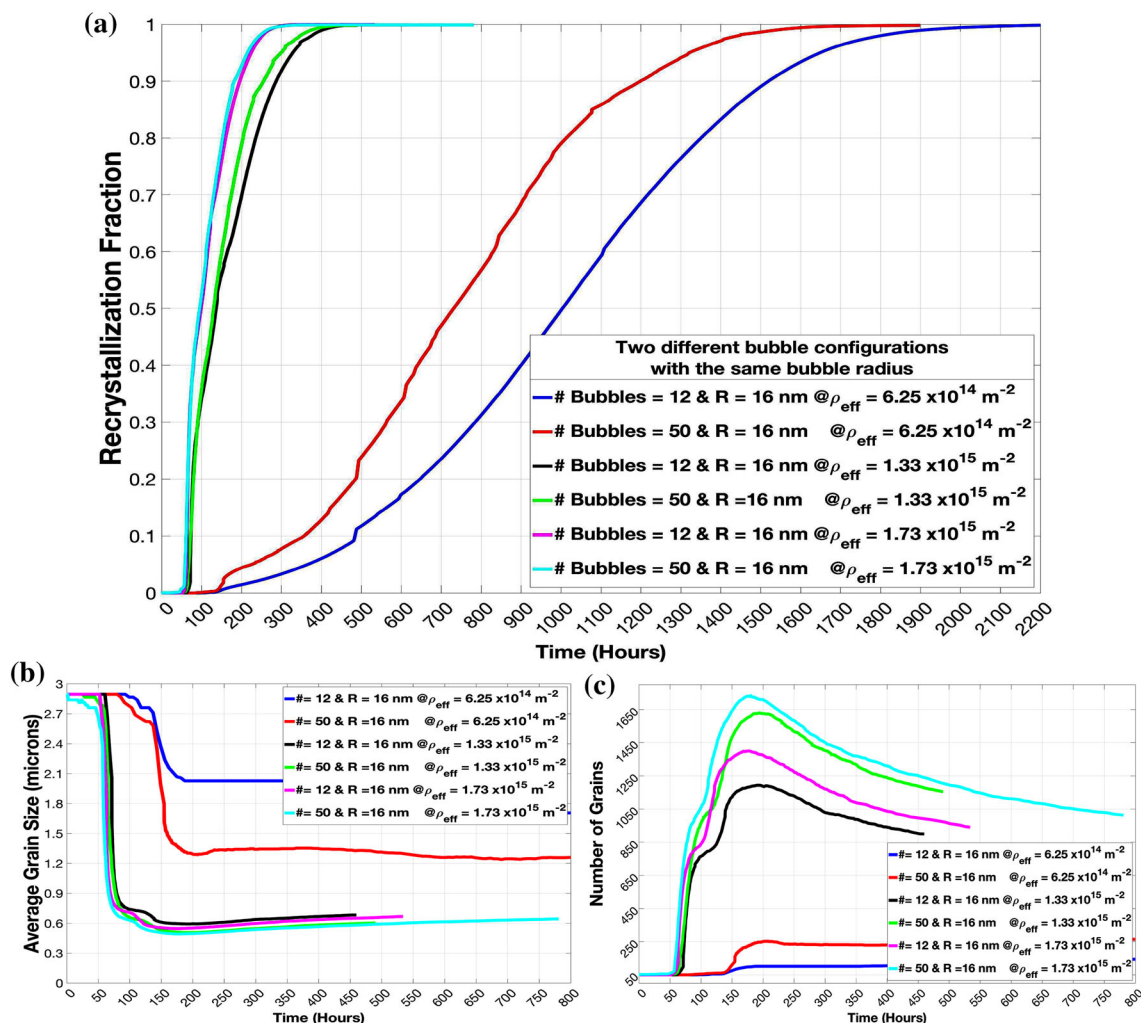
Fig. 8. Effect of bubble number density on (a) recrystallization rate in polycrystalline UO$_2$, (b) average grain size and (c) number of grains. For the same bubble radius and dislocation density, a higher number of bubbles leads to enhanced recrystallization kinetics. This enhancement is more apparent at lower dislocation densities.

theory and experiments. For polycrystalline UO$_2$ at 1200 K, the recrystallized average grain size was found to be on the order of 0.4 $\mu$m at a dislocation density of $\rho = 2.50 \times 10^{15}$ m$^{-2}$ (or equivalent to a burn-up of 72 GWd/tHM), which lies within the range of values reported in Refs. 1, 6, 33, and 34. We expect the agreement to be improved when we conduct full 3-D simulations.

The model can currently only account for the effect of grain size and temperature on the kinetics of HBS evolution. However, the model currently ignores the effect of grain size and temperature on the accumulation of dislocations. Nonetheless, this limitation can be alleviated by coupling the current phase-field model to a rate-theory model of irradiation damage. This will be the subject of future work. Moreover, in future studies, the heat and momentum balance equations will be coupled to the microstructure evolution equations to directly investigate the coevolution of the microstructure and the thermal and mechanical properties of HBS.

This can be accomplished in a straightforward manner using MOOSE.[36] Moreover, the nucleation of gas bubbles, bubble swelling, and gas release will be incorporated into the model. Furthermore, full 3-D simulations will be performed. This will provide a mechanistic mesoscale model capable of predicting HBS formation and evolution along with physical properties changes in current and future nuclear fuels.

# REFERENCES

1. T. Wiss and V.V. Rondinella, *Mater. Today.* 13, 24 (2010).
2. K. Nogita, K. Une, M. Hirai, K. Ito, K. Ito, and Y. Shirai, *J. Nucl. Mater.* 248, 196 (1997).
3. J. Spino, K. Vennix, and M. Coquerelle, *J. Nucl. Mater.* 231, 179 (1996).
4. J. Noirot, L. Desgranges, and J. Lamontagne, *J. Nucl. Mater.* 372, 318 (2008).
5. H. Matzke and M. Kinoshita, *J. Nucl. Mater.* 247, 108 (1997).
6. K. Nogita and K. Une, *J. Nucl. Mater.* 226, 302 (1995).
7. X.-M. Bai, M.R. Tonks, Y. Zhang, and J.D. Hales, *J. Nucl. Mater.* 470, 208 (2016).
8. K. Ahmed, X. Bai, Y. Zhang, B. Biner, Report No. 40046 Rev.0, (Idaho National Laboratory, Idaho, 2016).
9. N. Moelans, B. Blanpain, and P. Wollants, *Calphad.* 32, 268 (2008).
10. M.R. Tonks, A. Cheniour, and L. Aagesen, *Comput. Mater. Sci.* 147, 353 (2018).
11. P.C. Millett, A. El-Azab, S. Rokkam, M. Tonks, and D. Wolf, *Comput. Mater. Sci.* 50, 949 (2011).
12. Y. Li, H. Shenyang, X. Sun, and M. Stan, *Comput. Mater.* 3, 16 (2017).
13. K. Ahmed and A. El-Azab, Phase-field modeling of microstructure evolution in nuclear materials.*Handbook of Materials Modeling*, ed. W. Andreoni and S. Yip (Cham: Springer, 2018), .
14. L. Liang, Z.-G. Mei, Y.S. Kim, B. Ye, G. Hofman, M. Anitescu, and A.M. Yacout, *Comput. Mater. Sci.* 124, 228 (2016).
15. L. Liang, Z.-G. Mei, and A.M. Yacout, *Comput. Mater. Sci.* 138, 16 (2017).
16. J. Rest, *J. Nucl. Mater.* 326, 175 (2004).
17. M. Kinoshita, *J. Nucl. Mater.* 248, 185 (1997).
18. X. Donghua, B.D. Wirth, and F. Sci, *Techol.* 56, 1064 (2009).
19. M. Li, M.A. Kirk, P.M. Baldo, D. Xu, and B.D. Wirth, *Philos. Mag.* 92, 2048 (2012).
20. K. Elder and N. Provatas, *Phase-Field Methods in Materials Science and Engineering*, 1st ed. (Weinheim: Wiley, 2010), pp. 143–163.
21. P. Wollants, N. Moelans, and B. Blanpain, *Phys. Rev. B* 78, 024113 (2008).
22. N. Moelans, A. Godfrey, Y. Zhang, and D.J. Jensen, *Phys. Rev. B* 88, 054103 (2013).
23. M. Plapp, *Phys. Rev. B* 84, 031601 (2011).
24. N. Moelans, *Acta Mater.* 59, 1077 (2011).
25. L.K. Aagesen, Y. Gao, D. Schwen, and K. Ahmed, *Phys. Rev. E* 98, 023309 (2018).
26. K. Ahmed, J. Pakarinen, T. Allen, and A. El-Azab, *J. Nucl. Mater.* 446, 90 (2014).
27. K. Ahmed, C.A. Yablinsky, A. Schulte, T. Allen, and A. El-Azab, *Mod. Sim. Mater. Sci. Eng.* 21, 23 (2013).
28. P.V. Nerikar, K. Rudman, and T.G. Desai, *J. Am. Ceram. Soc.* 94, 1893 (2011).
29. H. Matzke and T. Inoue, *J. Nucl. Mater.* 91, 205 (1980).
30. J.B. Ainscough, B.W. Oldfield, and J.O. Ware, *J. Nucl. Mater.* 49, 117 (1973).
31. C.J. Permann, M.R. Tonks, B. Fromm, and D.R. Gaston, *Comput. Mater. Sci.* 115, 18 (2016).
32. K. Ahmed, M. Tonks, Y. Zhang, B. Biner, and A. El-Azab, *Comput. Mater. Sci.* 134, 25 (2017).
33. H. Xiao, C. Long, and H. Chen, *J. Nucl. Mater.* 471, 74 (2016).
34. K. Une, K. Nogita, S. Kashibe, and M. Imamura, *J. Nucl. Mater.* 188, 65 (1992).
35. R. Bullafi, W. Carter, and S. Allen, *Kinetics of Materials*, 1st ed. (Cambridge: Wiley, 2005), pp. 459–485.
36. L.K. Aagesen, D. Schwen, K. Ahmed, and M. Tonks, *Comput. Mater. Sci.* 140, 10 (2017).